We are IntechOpen,
the world's leading publisher of Open Access books
Built by scientists, for scientists

6,900
Open access books available

185,000
International authors and editors

200M
Downloads

154
Countries delivered to

Our authors are among the

TOP 1%
most cited scientists

12.2%
Contributors from top 500 universities

CLARIVATE ANALYTICS
BOOK CITATION INDEX
INDEXED

WEB OF SCIENCE™

Selection of our books indexed in the Book Citation Index
in Web of Science™ Core Collection (BKCI)

Interested in publishing with us?
Contact book.department@intechopen.com

Plasma-Assisted Combustion

Siyin Zhou, Haiqing Wang, Wansheng Nie and
Xueke Che

Additional information is available at the end of the chapter

Abstract

As a promising technology, plasma-assisted combustion (PAC) has attracted many researchers to explore the effect of PAC on improving the combustion in propulsion devices, such as scramjet, detonation engines, internal engines, and so on. In this chapter, we aim to exhibit the influence of quasi-DC discharge plasma on the operating performance of scramjet combustor and find the internal mechanisms, which may contribute to the development of PAC technology in supersonic combustion. For case one, a plasma filament is generated upstream of fuel jet through quasi-DC discharge in a scramjet combustor; for case two, the plasma is formed across the backward facing step of a flame holding cavity to improve the flame stabilization of the cavity in the scramjet combustor. The two cases are investigated in detail through three-dimensional numerical simulation based on the dominant thermal blocking mechanism. Important parameters including temperature distribution, separation zone, water production, stagnation pressure loss, combustion efficiency, cavity drag, mass exchange rate, and cavity oscillating characteristics are obtained and analyzed. It shows that the quasi-DC discharge plasma does benefit for the improvement of the combustion in a scramjet combustor.

Keywords: quasi-DC discharge, plasma-assisted combustion, supersonic combustion, scramjet, transverse fuel jet, cavity, numerical simulation

1. Introduction

As one of the qualified candidates for hypersonic propulsion system, scramjet combustor has attracted a large amount of attention all over the world. As is now well known, realizing high efficiency and steady combustion in a supersonic combustor always remains as a critical issue for scramjet engines. Numerous researches have indicated that the additions of cavity in combustor and the transverse fuel injection upstream of the cavity can promote the stabilization of

combustion and flame [1–3]. Whereas, it is difficult yet for the fuel to reach properly mixing within the supersonic flow by the mechanical methods [4, 5]. Moreover, it is a great challenge for matching the transverse fuel jet up with the cavity under off-design condition [4]. Furthermore, certain stagnation pressure loss will appear using the approaches. Taken all account, some new methods are imminently needed for keeping stable and highly efficient combustion in combustor with the least penalties adding to the flowfield.

It is rather promising to adopt a discharge plasma for supersonic flow and/or combustion control in aerospace field [6–8]. It has been widely considered that plasma-assisted combustion is one of the most promising approaches for enhancing ignition and combustion in the environment of scramjet combustion [4, 6, 9]. As a further promising method, there are three advantages, that is: rapid response, less inertia, and flexibility [10]. Former studies clearly show that the quasi-DC discharge plasma can availably modify supersonic flow in a controllable manner among the discharge plasma mentioned above [8, 11], whereas the DBD plasma is commonly used in low-speed flow environment [12, 13]. If we can combine the quasi-DC discharge plasma with cavity and transverse fuel jet together, some new phenomena will surely appear, which may help in the improvement of combustor performance.

There in three primary mechanisms of the plasma effect on flow and combustion can be summarized: (1) momentum transfer, (2) fast local ohmic heating of the medium, and (3) active particles [6, 7, 14]. Ignoring the magnetic field, the mechanism of quasi-DC discharge plasma affecting a supersonic flow is mainly its fast local heating rather than the electrostatic force (i.e., the momentum transfer mechanism) [10, 15, 16].

This chapter aims at investigating the changes of the fuel jet, cavity, and whole scramjet combustor led by the quasi-DC discharge plasma based on the dominant thermal blocking mechanism. Here, a short cavity downstream of a fuel jet orifice is considered in order to simulate the combustor flowfield more realistic. The plasma is set as a controllable heat source. The k-ω shear stress transport (SST) model together with finite rate chemical reaction model is used simulating the turbulent flow and combustion. The flow structures, equivalent ratio, product distribution, stagnation pressure, and combustion efficiency in the combustor are all obtained and analyzed using the 3D numerical simulation which can acquire some data that are difficult to measure in experiments.

2. Case one—effect of plasma on fuel jet

2.1. Numerical methods

2.1.1. Plasma model and its configuration

By applying a high voltage across the anode and cathode, a bright plasma filament appears above the two electrodes. With the impacting of incoming flow, the plasma occurs not only between the two electrodes but also several centimeters downstream on the wall [10]. In consideration of the oscillation character of its electrical parameters and mean temperature in

the discharge path, this type of discharge plasma is called "quasi-DC discharge plasma." However, it is a type of low temperature arc plasma in fact. The main properties of quasi-DC discharge plasma are described in [10–12, 15].

As depicted in **Figure 1**, the domain of quasi-DC discharge plasma filament is simplified as a cuboid region presented in red dashed lines for simulation based on its appearance. In **Figure 1**, the symmetric plotted line indicates that the cathode and anode are symmetrical for the central line of combustor wall and so does the plasma filament.

Because the quasi-DC discharge plasma releases a large amount of heat concentrated in its discharge path, the discharge path goes into very hot. This high temperature domain (i.e., the discharge path) obstructs the supersonic inflow due to a thermal blocking occurred. Hereby, the quasi-DC discharge plasma behaves as a virtual blockage in the high speed flow of scramjet combustor, which is called as "the dominant thermal blocking mechanism" [17]. On the foundation of dominant thermal blocking mechanism, the individual plasma filament can be simulated as a volumetric heat source [10, 12].

Generally speaking, the plasma input power and the effective heat power that transfers into circumambient gas are quite different. Besides, the percentage of loss commonly varies with the power supply and environment, so it is not a suitable way to use the plasma input power as the heat source value of quasi-DC discharge plasma in simulation. In order to straightforwardly describe the plasma heat strength, the average temperature of the plasma zone is acquired by using the numerical simulation here. This way is feasible when the average temperature of the plasma zone is within a reasonable range [10, 16, 18, 19]. Hence, based on the thermal blocking mechanism, a certain temperature which denotes the actuating strength (i.e., the input power) is specified for the plasma filament domain when the actuator works.

The electrodes are flush mounted and do not have influence on the main flow themselves. The length and the section dimensions of individual plasma filament heat source are 20 mm length and 3×3 mm, respectively. The plasma filament locates 40 mm upstream of the fuel orifice center. Besides, it is generated near the wall in the center of the combustor, which means the symmetric plane of plasma filament is within the symmetric xy-plane of combustor. The quasi-DC discharge plasma working under a pulsed mode shows better performance than a continuous mode [19], so a plasma control frequency $F_c = 8$ kHz with duty cycle ratio $D = 2/5$ is chosen here. And $T_{pl} = 2500$ K is specified as an optimal actuating strength.
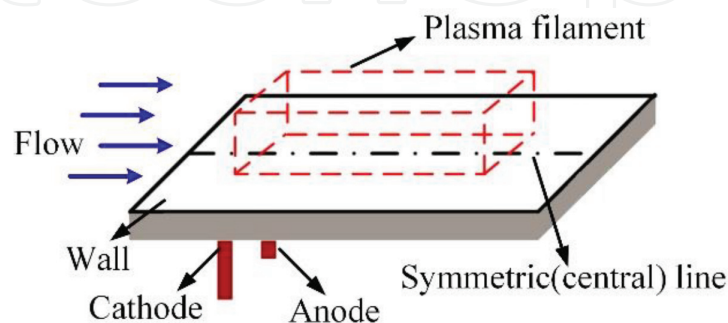

Figure 1. Computed configuration of quasi-DC discharge plasma in case one.

2.1.2. Governing equations, physical models, and numerical schemes

The unsteady Reynolds averaged 3D Navier-Stokes equations (URANS) with the k-ω SST two equation turbulence model [20] and four species (H_2, O_2, N_2, and H_2O) conservation equations are used as the governing equations of flow and combustion. The thermal conductivity of every species remains as constant and the mixture thermal conductivity is calculated using ideal gas mixing law. Based on the perfect gas assumption, it can be seen that the mixing gas satisfies the local thermodynamics equilibrium hypothesis and follows the state equation:

$$P = R_0 T \sum_{i=1}^{N_s} \frac{\rho_i}{W_i} \qquad (1)$$

here, R_0 = 8.314 J/ (mol·K) is the gas constant. The specific heat capacity c_{pi} of species i is derived from a piecewise polynomial as follows:

$$c_{pi} = a_{1,i} + a_{2,i}T + a_{3,i}T^2 + a_{4,i}T^3 + a_{5,i}T^4 \qquad (2)$$

where the coefficients can be found in [21]. The k-ω SST two equation turbulence model is used here because of its well behave in separation flow and free shear flow. Based on the Boussinesq assumption, viscosity coefficient $\mu = \mu_l + \mu_t$, where μ_l is the laminar viscosity coefficient and μ_t is the turbulence viscosity coefficient. μ_l can be received from the Sutherland law, whereas μ_t is received from the k-ω SST model.

$$\mu_l = \mu_{\text{ref}} \left(\frac{T}{T_{\text{ref}}} \right)^{2/3} \frac{T_{\text{ref}} + S}{T + S} \qquad (3)$$

where μ_{ref} is the reference viscosity coefficient under corresponding reference temperature T_{ref} and S is the Sutherland constant which can be got from **Table 1**.

Since this study focuses on the qualitative effect of plasma on the fuel jet and the scramjet combustor, the finite rate chemical model with the single step H_2/O_2 combustion kinetics model is applied. The reaction rate constant is derived from the Arrhenius formula. Hence, the computational time can be saved much and the well combustion flowfield can be obtained, too. The relevant parameters of H_2/O_2 one-step chemical model are shown in **Table 2**.

In order to capture the shock waves and other complex fluid structures better, the convective fluxes are evaluated using the advection upstream splitting method (AUSM) [22] with the

	T_{ref} (K)	S (K)	μ_{ref} (kg/m·s)
H_2	273.11	96.67	8.411×10^{-6}
O_2	273.11	138.9	1.919×10^{-5}
H_2O	416.67	861.11	1.703×10^{-5}
N_2	273.11	106.67	1.663×10^{-5}

Table 1. Parameters in Sutherland law.

Equation	Pre-exponential factor	Temperature index	Activity energy [J/kg·mol]
$H_2 + 0.5O_2 \leftrightarrow H_2O$	9.87E + 8	0	3.1E + 7

Table 2. H_2/O_2 one-step chemical model.

second-order upwind approach at same time. The viscous fluxes are evaluated by using the second-order central differential scheme. Because the transport process of multispecies and the reaction both exist in the flowfield, a modified LU-SGS implicit method [23] is adopted for temporal integration.

2.1.3. Computational zone and boundary conditions

Figure 2 shows the entire computational domain which is the half of scramjet combustor together with a short cavity and a fuel jet orifice. The inlet of combustor is located at $x = 0$ mm, which is 33.064 mm high and 44 mm wide. The upper wall angle is set as 1° to prevent thermal block. For avoiding the interaction between multifuel jets, there is only one single fuel orifice arranged at the symmetric plane of combustor, which locates at 60 mm downstream of the inlet. The distance between the fuel orifice center and the leading edge of downstream cavity is 10 mm, which can strengthen the resisting back pressure capability. And a short cavity is adopted here with rear edge angle 45°, length 56 mm, width 44 mm, and depth 8 mm, respectively. Instead using a circular fuel orifice, a 1.772 mm × 1.772 mm square cross section orifice is adopted to acquire high-quality mesh, which has the same cross section area as a 2 mm diameter circular orifice.

The grids number is largely reduced by setting the symmetry face (*xy*-plane) of combustor as a symmetry boundary condition. In order to improve the quality of computational grids, the whole domain is divided into six parts to make all grids in structured type, except for the rear part of the cavity with unstructured grids. All grids aspect ratio and equisize skew are within 8 and 0.54, respectively. Grids are refined in key zones, such as the plasma domain, fuel orifice, wall, and shear layer. Besides, grids in zones with relatively large pressure gradient and the boundary layer are refined using adaptive mesh refining method based on the initial simulation
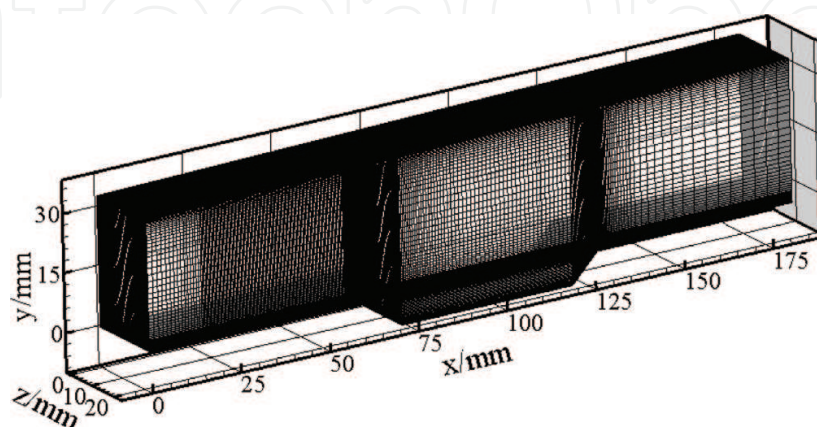

Figure 2. Computational domain and grids of the combustor.

results. After comparing the results of different grids size, a mesh scheme which consists of 955,166 cells in the whole computational zone is chosen, and it can be proved when the grids size increases, the flowfield remains almost unchanged all the same.

The entire computational domain is divided into 32 subdomains, and all assignments are completed by parallel computation on HP senior workstation, which takes about 320 h to obtain a convergence result. The inflow conditions in computation are as follows: Ma = 2.2, static pressure P = 101 kPa, static temperature T = 823 K, and boundary layer thickness δ = 2.0 mm. In order to identify product water, dry air is set as the inflow (the mass fraction of oxygen and nitrogen are Y_{O2} = 23.3%, Y_{N2} = 76.7%, respectively). Here, hydrogen is used as fuel which is perpendicularly injected into the main flow at sonic speed. The parameters of fuel injection at the outlet of fuel orifice are given as: static pressure P_{jst} = 334 kPa, stagnation pressure P_{j0} = 0.6 MPa, and stagnation temperature T_{j0} = 290 K. At the exit boundary, the supersonic extrapolation condition is used. Besides, symmetry condition is used in central xy-plane (z = 0) for decreasing the calculation cost. There is no slip and adiabatic conditions, which are specified on the upper, bottom, and lateral walls of combustor including the cavity walls.

2.1.4. Simulation validation

The ability of our numerical methods for simulating the multispecies reaction flow field of the scramjet combustor with a cavity has been validated and can be found in [14, 18].

2.2. Results and discussion

Three representative times are selected during one plasma control cycle for comparison after computation converged. The end of the actuator duty time (t = 2/5T_c, where T_c is the period of one plasma control cycle), a certain time of the actuator free time (t = 4/5T_c) and the end of a whole plasma control cycle (t = T_c) are named A, B, and C, respectively.

2.2.1. Temperature and wall pressure distribution of the jet flowfield

The temperature distribution on the symmetric xy-plane of combustor is shown in **Figure 3**. It can be seen that the relatively high temperature zone appears mainly in the cavity when there is no plasma actuator arranged. But it moves downstream with the actuator working. The local temperature of the near wall downstream and the rear part of the cavity increases distinctly, which means the combustion centrality zone moves downstream. Besides, the lower temperature zone which denotes the fuel jet flow (i.e., the deep blue zone in **Figure 3**) prominently shrinks as the actuator works. However, the area of the lower temperature zone extended gradually at time B and C compared with time A. The unsteady phenomena should be due to the high heat nature of quasi-DC discharge plasma, which transfers its heat to the fuel jet resulted in changing the combustion zone downstream.

The distribution of wall pressure near the fuel orifice on the symmetric plane of the combustor is shown in **Figure 4**, which is normalized by the value of the static pressure of inflow at the inlet. Compared with no plasma case, the positions that pressure starts to rise at different times
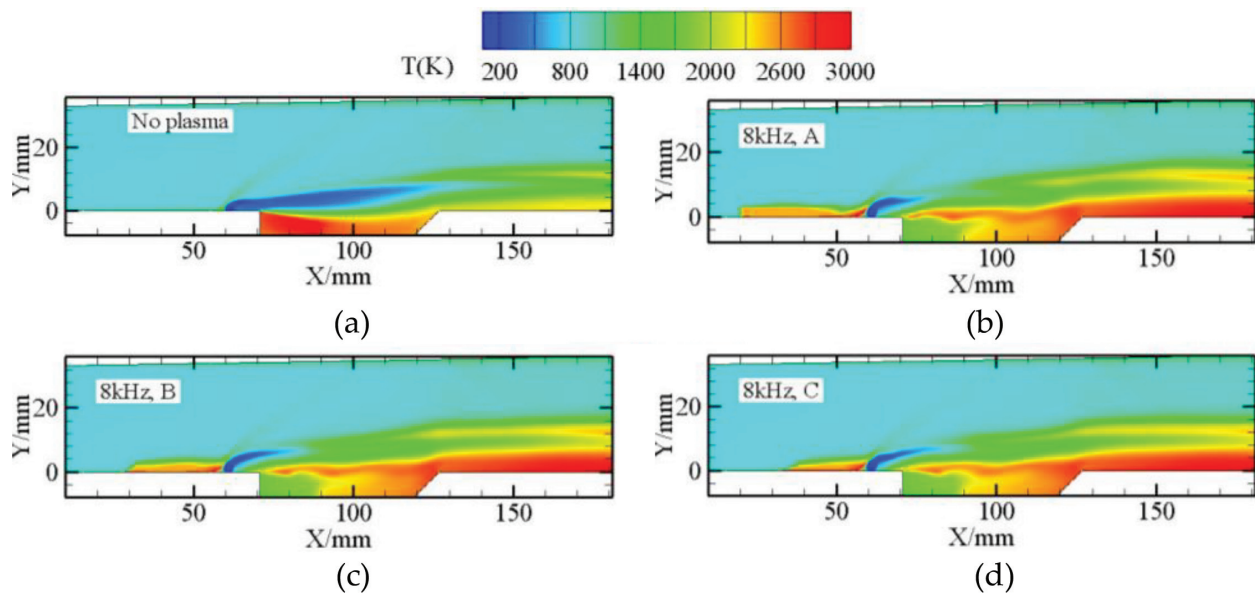
Figure 3. Contours of temperature on the symmetric *xy*-plane of combustor. (a) Plasma off. (b) Plasma on, time A. (c) Plasma on, time B. (d) Plasma on, time C.
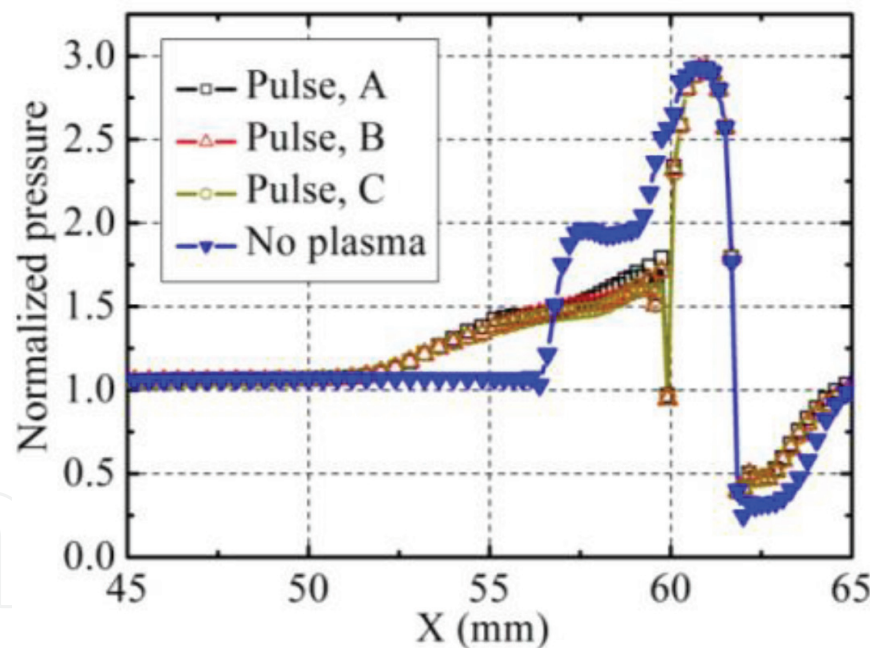

Figure 4. Wall pressure distribution on the symmetric plane.

move upstream from 56.6 to 52 mm due to the effect of plasma, which indicates the separation shock wave induced by the fuel jet moves upstream. And the first pressure peak decreases from 2.0 to 1.7, because of the weakening of the fuel jet induced shock on the symmetric plane. The results above are similar to the previous studies on nonreaction flow combustor [19]. More details indicate that the first pressure peak of time A is a bit higher than time B and C, but time B equals time C, which is due to the plasma control cycle too

short for flow response and the duty cycle ratio also comparatively large in the flow condition here. Hence, the influence of plasma on the shock will be observed a little latter due to an inertia influence. Nevertheless, the effect of plasma on the shock wave for three typical times is highly similar on the whole.

Because the separation zone upstream of the fuel orifice is primarily controlled by the separation shock wave, the size of this separation zone can be regulated by changing the location of the separation shock wave. On the one side, this zone behaves as an main ignition zone which can provide a high temperature and low flow speed environment in the scramjet combustor. On the other side, it will bring in certain pressure loss to the combustor. Hence, we can make use of the separation zone upstream of the fuel orifice by means of using the plasma with proper control parameters.

2.2.2. Characteristics of fuel mixing and combustion

For the sake of determining the fuel mixing quality, the five cross-sectional planes distributed in equivalent ratio along the flow direction are given, as shown in **Figure 5**. The fuel jet arises with the actuator working, resulting in fuel decreasing near the wall including the bottom wall of the cavity. Whereas, the distribution shape of fuel in the cross-sectional planes varies from a distribution narrow and long profile into a circular profile in the upper space, which shows that the process of fuel spreading into the main supersonic flow is enhanced resulted from the plasma. Furthermore, the fuel distributions at time A are nearly the same as at time C, which is also correlated to the inertial effect mentioned above.

In **Figure 6**, the distribution of product water is shown. In order to distinguish the extent of product water between time A and C easily, the iso-surfaces of both are plotted by combining the half parts of them together as shown in **Figure 6(b)**. Similar to the changes in **Figure 5**, more water is generated in the upper space due to plasma. Contrasted with the case without plasma actuator, the iso-surface of water expands much in its center and shrinks near the combustor wall especially downstream of cavity. These above should be attributed to the change of fuel jet spread, as given in **Figure 5**. Compared time A with C, the only distinction is a little more water formed at time A, which indicates that the combustion becomes weaker in the free time of a plasma control cycle.
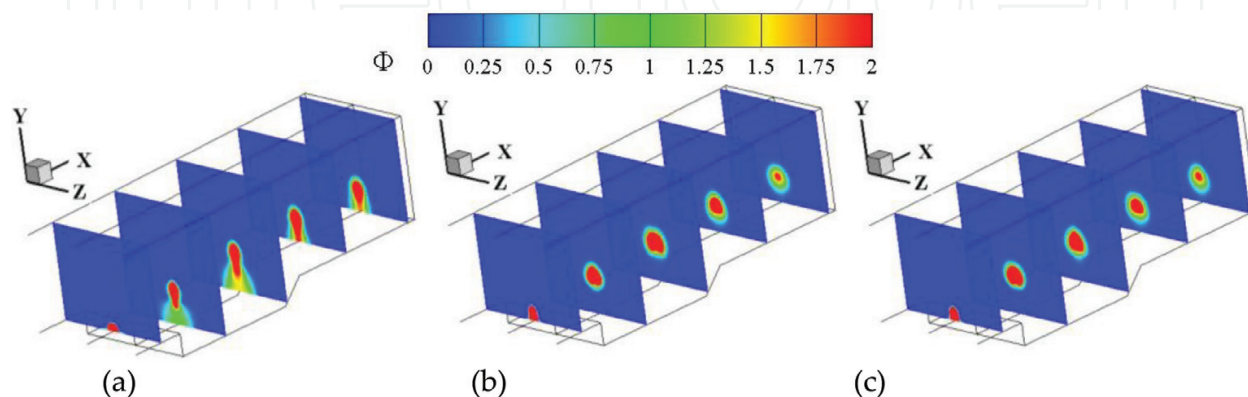

Figure 5. Distribution of equivalent ratio in cross-sectional planes. (a) Plasma off. (b) Plasma on, time A. (c) Plasma on, time C.
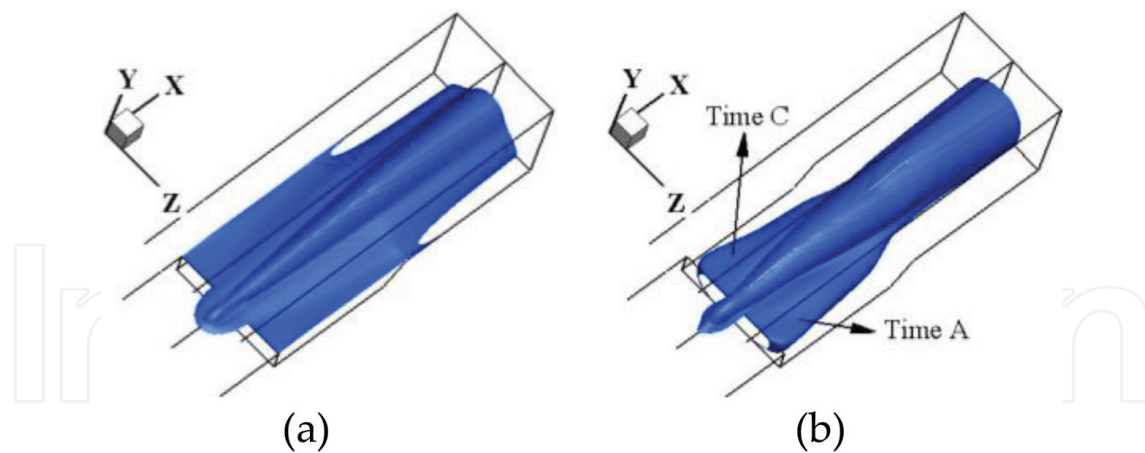
Figure 6. Iso-surfaces of product water, $Y_{H2O} = 0.015$. (a) Plasma off. (b) Plasma on.

It can be seen that the fuel entrainment into the cavity is decreased and the combustion in cavity becomes weaker due to the plasma, as given in **Figures 5** and **6**.Whereas, the two figures also show that more fuel penetrates into the supersonic air flow, so the mass exchange between the inside cavity and its outside is enhanced due to the plasma. Hence, the plasma improves the fuel mixing above the cavity prominently, which can also be realized as the calculation results of combustion efficiency in Section 2.2.4.

2.2.3. Combustor stagnation pressure

The stagnation pressure recovery coefficient can indicate the pressure loss in a combustor, so it is an important index. When the stagnation pressure recovery coefficient goes up, the capability of combustor outflow will be enhanced. So, it is defined as the ratio of combustor outlet stagnation pressure to inlet stagnation pressure [24]. In fact, calculating the mass flow weighted mean stagnation pressure can gain the stagnation pressure in a cross section.

$$\eta_{p_0} = \frac{\overline{p}_{0\_outlet}}{\overline{p}_{0\_inlet}} \tag{4}$$

where η_{p0} and $\overline{p}_0$ are the stagnation pressure recovery coefficient and the combustor stagnation pressure, respectively.

$$\overline{p}_0 = \frac{\int p_0 \overline{\rho} u \, dy}{\int \overline{\rho} \, dy} \tag{5}$$

where u and $\overline{\rho}$ are the flow velocity across a certain plane and the density of selected plane, respectively. Based on above, we get the stagnation pressure loss coefficient:

$$\eta_{p_0,\, loss} = 1.0 - \frac{\overline{p}_{0\_outlet}}{\overline{p}_{0\_inlet}} \tag{6}$$

The calculated data about the stagnation pressure are given in **Table 3**. In order to analyze the tendency of stagnation pressure loss coefficient further, the average stagnation pressure at the

outlet is replaced by the average stagnation pressure at different positions, as shown in **Figure 7**. At the actuator working time or even at the free time, the stagnation pressure loss can both be increased due to the plasma, as given in **Table 3**. In (7), the relative change rate of η_{p0} is defined to realize the variation degree of the stagnation pressure recovery coefficient.

$$\varepsilon_i = \left| \frac{\eta_i - \eta_b}{\eta_b} \right| \times 100\% \tag{7}$$

where η_i is the stagnation pressure recovery coefficient of a certain case and η_b is the base case.

In **Figure 7**, the difference of stagnation pressure loss between plasma cases is shown where no plasma case enlarges along the flow direction (x-direction). At time A, B, and C, the relative change rate of stagnation pressure recovery coefficient at outlet point are 3.7, 3.1, and 3.4%, respectively, which indicates that the stagnation pressure loss varies little during a whole plasma control cycle and the loss is relatively little. The reasons resulted in these changes are

Index of performance	Case			
	Plasma off	Plasma on, time A	Plasma on, time B	Plasma on, time C
P_{0_inlet} /Pa	1,098,093			
P_{0_outlet} /Pa	916,532	882,270	888,143	885,268
η_{p0}	0.83466	0.80346	0.80880	0.80619
$\eta_{p0,loss}$	0.16534	0.19654	0.19120	0.19381

Table 3. The inlet mean stagnation pressure P_{0_inlet}, outlet mean stagnation pressure P_{0_outlet}, stagnation pressure recovery coefficient $\eta_{p0\ z}$, and stagnation pressure loss coefficient in the combustor.
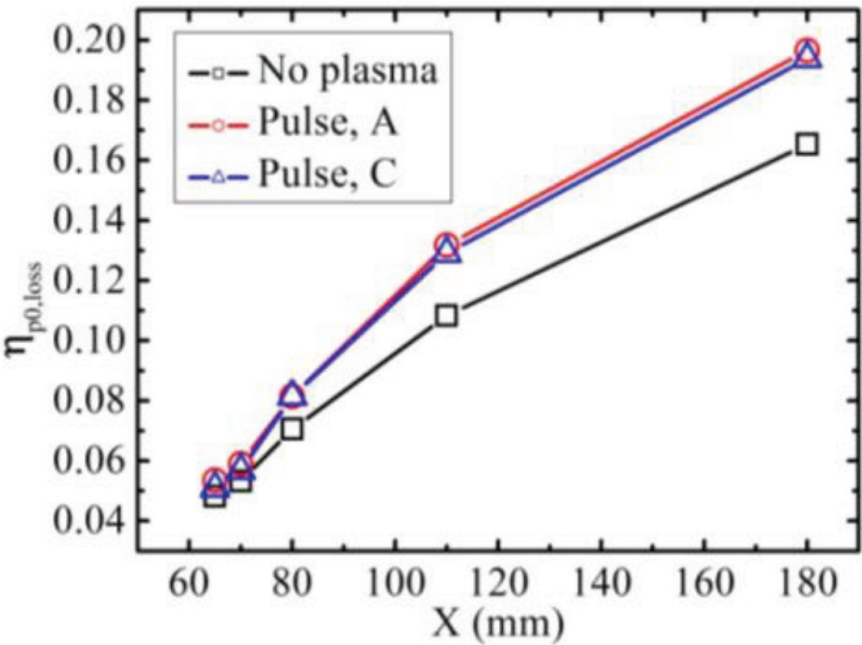

Figure 7. Distribution of the stagnation pressure loss coefficient.

in three aspects: (1) the strength of separation shock upstream of the jet is changed due to plasma as mentioned above, which will affect the stagnation pressure distribution; (2) the quasi-DC discharge plasma behaves as a virtual blockage in supersonic flow resulted in new shock waves or compression waves forming. Then, the pressure loss is increased; (3) the heat release from combustion can result in the stagnation pressure decreasing. Hence, the increase of stagnation pressure loss in the combustor is correlated to all the changes in flowfield which is due to the comprehensive effect mentioned above. To ensure the maximal combustion efficiency while keeping the stagnation loss as little as possible, the optimal design is important. So the calculation of combustion efficiency is essential to choose the proper plasma actuator parameters.

2.2.4. Combustion efficiency downstream of the fuel orifice

The combustion efficiency η_c is commonly denoted by the amount of combustion product. Thus, the amount of water is employed [24]:

$$\eta_c = \frac{(\dot{m}_{H_2O,X} - \dot{m}_{H_2O,I})/W_{H_2O}}{\dot{m}_{H_2}/W_{H_2}} \qquad (8)$$

where $\dot{m}_{H_2O,I}$ is the mass flow rate of water at inlet cross section and $\dot{m}_{H_2O,x}$ is x-direction cross section, respectively. $\dot{m}_{H_2}$ and W_i are the mass flow rate of hydrogen and the mole mass of specie i, respectively. And dry air is assumed at the inlet in the simulation $\dot{m}_{H_2O,I} = 0$.

Figure 8 plots the distribution of combustion efficiency in x-direction. At both time A and C, the rise rates of combustion efficiency go into larger along x-direction. At the outlet, η_c reaches 0.81341, 0.76008, and 0.60278 for time A, C, and no plasma case, respectively. Namely that η_c at time A and C are 1.35 and 1.26 times of no plasma case. As a result, the quasi-DC plasma does obviously improve the combustion in combustor on the whole level, as shown in **Figure 8**, even if the most water forms in the upper space rather than in the cavity. But the η_c at time A and time C are almost same. From **Figure 6**, the increase of combustion efficiency can also be realized, which indicates that the mixing performance of the fuel jet in scramjet combustor is improved due to the quasi-DC discharge plasma.

In order to define the cost to effectiveness of quasi-DC plasma, it is calculated in value $E_f = 0.00811$ for the ratio of deposited plasma energy to the increased combustion heat release. Accordingly, for improving the combustion of scramjet combustor, the quasi-DC plasma shows good capability as costing a little.

2.3. Conclusions

The main results in this section are as follows: (1) The distribution of relatively high temperature zone moves downstream prominently due to the heat release from the quasi-DC discharge plasma. The separation shock wave induced by the fuel jet is partly weakened and moves upstream due to the plasma, which can regulate the size of recirculation zone upstream of the fuel orifice. (2) The fuel jet moves upward integrally resulted from the plasma heating effect. The fuel spread wider along the spanwise and penetrates into the leading flow deeper,
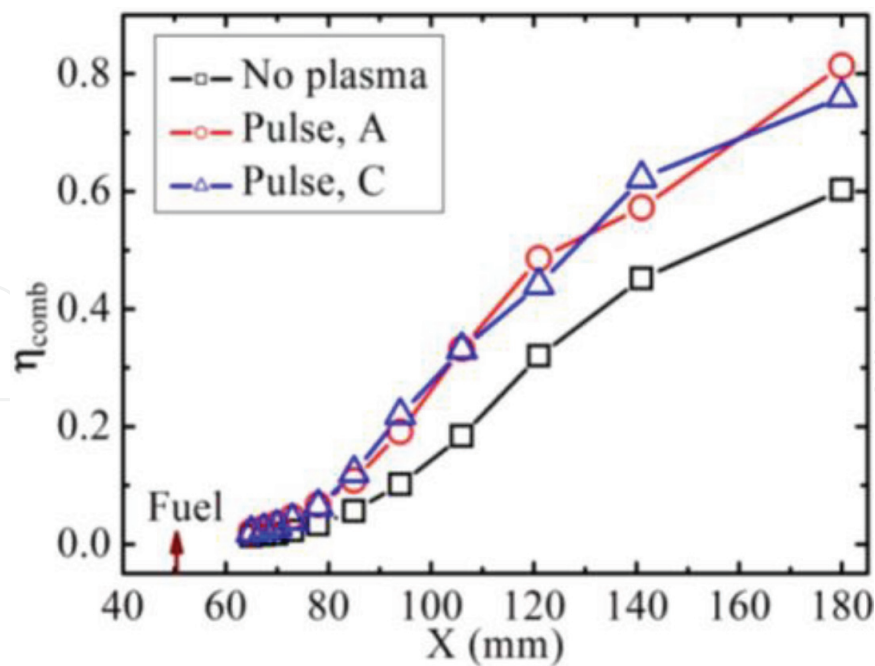
Figure 8. Distribution of combustion efficiency downstream of fuel orifice.

resulting in the cross-section shape of the fuel jet varying from a narrow and long profile to a circular profile. Because of the variation of fuel mixing, in the upper space, more water forms while less appears near the wall compared with the case without plasma. (3) The stagnation pressure loss of combustor increases a little as actuator works, but the combustion efficiency in the combustor rises obviously. These above can be summarized as the comprehensive effects of flow structure changes caused by the plasma, including waves induced and heat transfer. Since it is negligible for the relative change of stagnation pressure recovery coefficient in the actuator working cases, and the ratio of deposited plasma energy to the increased combustion heat release is very little, it can be obtained that the quasi-DC discharge plasma can make more benefits than penalties for the scramjet combustor, when proper adopting control parameters of the plasma actuator.

3. Case two—effect of plasma on cavity

3.1. Plasma model

On account of the direction of the quasi-DC discharge path for the inflow, the discharge modes include two types: longitudinal mode and transversal mode [12]. In case one, the quasi-dc discharge operates under transversal mode, while in case two, a longitudinal mode is adopted for the configuration. As shown in **Figure 9**, there are five anodes set upstream of the backward wall of cavity, while in the bottom wall of cavity the five cathodes are set. The five pairs of identical electrodes are arranged parallel and symmetrically. Besides, the flow will not be disturbed directly resulted from all the electrodes flush mounted in the wall. A filament plasma forms when applied a high voltage (generally 150–1200 V) between anode and cathode, which
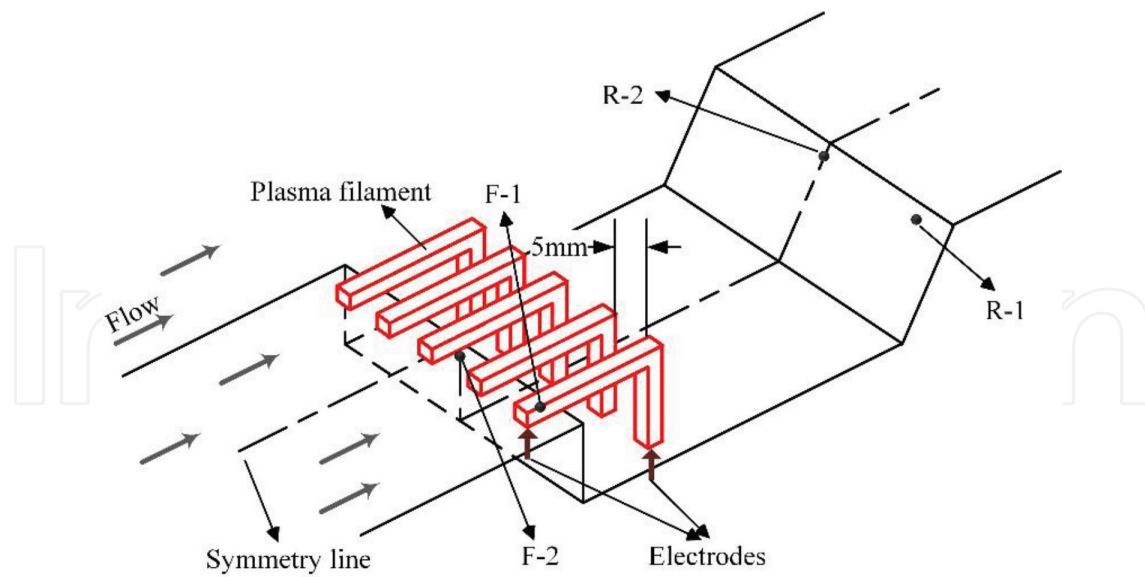
Figure 9. The schematic of plasma filaments in the cavity.

acts as strongly oscillating and bright and looks like an inverted "L" crossing the backward wall of cavity. Since the major heat energy of the quasi-DC discharge plasma focuses on the bright filament domain [10, 25], the filament plasma domain can be established in such a simplified shape as given in **Figure 9**.

Just like the way given in case one, every quasi-DC plasma filament is dealt as a volumetric heat source. To represent the plasma heat strength reasonably, the mean temperature of the plasma domain T_{pl} is specified in this simulation too. Considering the real size of the plasma filament, all the heat source is modeled with a section of dimensions 3×3 mm. the distance between the backward wall and left side of plasma filament upstream of cavity is 6 mm as depicted in **Figure 9**. While the distance between the backward wall and the right side of plasma filament downstream of cavity is 25.5 mm. Based on the previous research, $T_{pl} = 3000$ K is specified as the actuating strength, and five actuators work together in a pulsed mode with plasma actuation frequency $F_c = 5$ kHz and duty cycle $D = 1/5$. In this case, all configurations (e.g., combustor, cavity) and simulation conditions are identical to those used in case one, except for the plasma. Therefore, the numerical methods, including physical models, numerical schemes, computational zone, etc., could be found in Section 2.1.

3.2. Results and discussion

Three representative times are chosen from one plasma cycle, which consists of the later actuator free duration and the actuator working duration, for comparison after computations converged. In the simulation, the duration of one plasma cycle is $T_c = 200$ μs. The end of an actuator working duration $t = 1/5T_c$, $t = 3/5T_c$, and the end of a cycle $t = T_c$ are named A, B, and C, respectively.

3.2.1. Typical parameters distribution of cavity flowfield

The Mach number distribution of local cavity flowfield on the symmetrical xy plane is shown in **Figure 10**. A distinct shear layer forms upon the cavity mouth and develops toward the
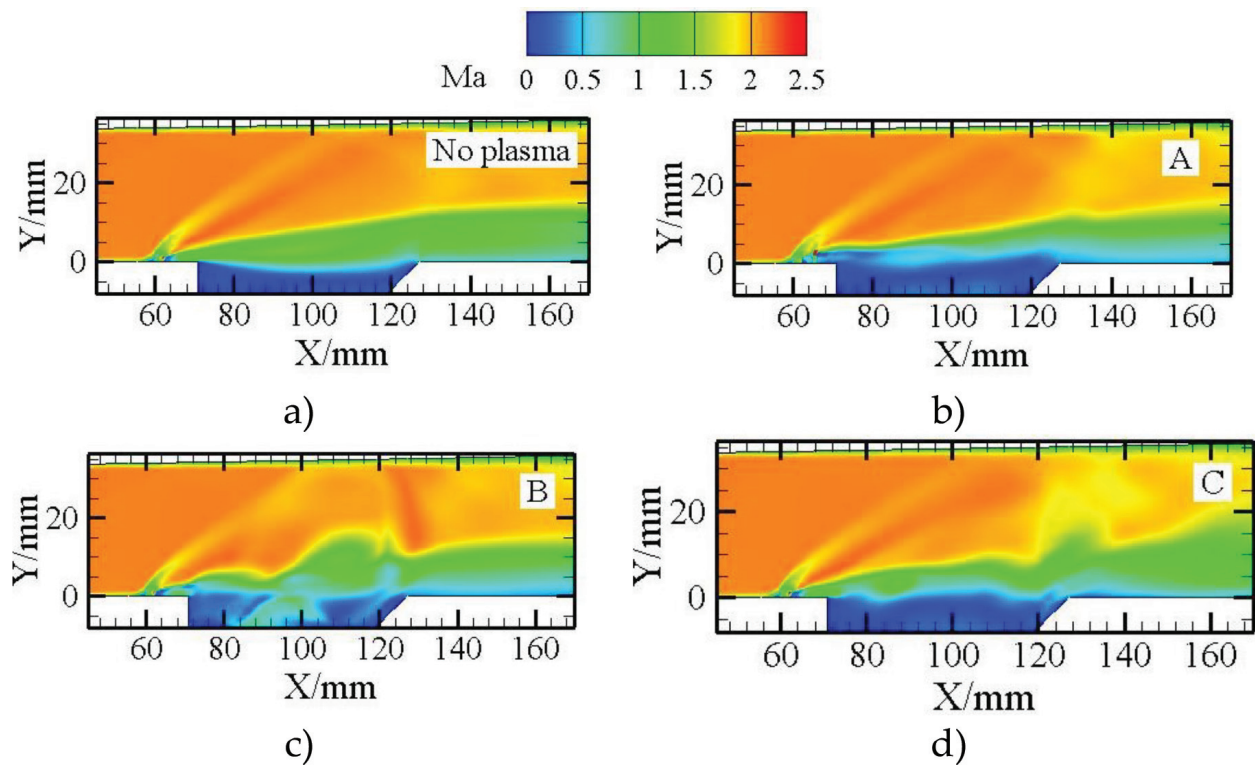
Figure 10. Mach number distribution: (a) no plasma; (b) with plasma, time A; (c) with plasma, time B; (d) with plasma, time C.

main flow, which is well known as the typical combustion flowfield of cavity. Contrasted with the flowfield of the no plasma case, the cavity shear layer fluctuates abruptly, particularly in the y direction. And it develops unsteadily resulted in the division of cavity recirculation zone at time B, as depicted in **Figure 10c**. Resulted from the plasma observed the Mach number distribution from time A to C, the main flow velocity downstream of the cavity decreases to a certain degree. On the whole, the oscillation phenomenon of cavity shear layer strengthens firstly and then weakens in pace with the plasma cycle.

Owing to the periodic heat release from the plasma filaments and the thermal blocking functions, the plasma filaments behave as five knives cut the cavity shear layer. Hence, the mass transportation process will be disturbed by this "cutting" effect, and the moving direction of original shear layer has to be changed also. And then, the turbulence intensity and vorticity magnitude both are increased, so the fuel and air existing around the original shear layer can exchange through the cavity mouth more easily. Furthermore, the combustion enhancement downstream or over the cavity causes the decrease of local flow velocity, which results in the rise of local static pressure and blocks the incoming flow.

Figure 11 presents the distributions of wall pressure near the rear edge of cavity on $z = 0$ and $z = 16$ mm plane. The pressure value on y-axis is normalized by the inflow static pressure. Being the same as the Mach number in **Figure 10**, the plasma influence on the wall pressure is strong and unsteady. On $z = 0$ mm plane, the pressure peaks of both time A and C move upstream compared with the no plasma case, which are shown in **Figure 11a**). At time A, its peak value is nearly equal to the case without plasma, and decreases more gently from its peak
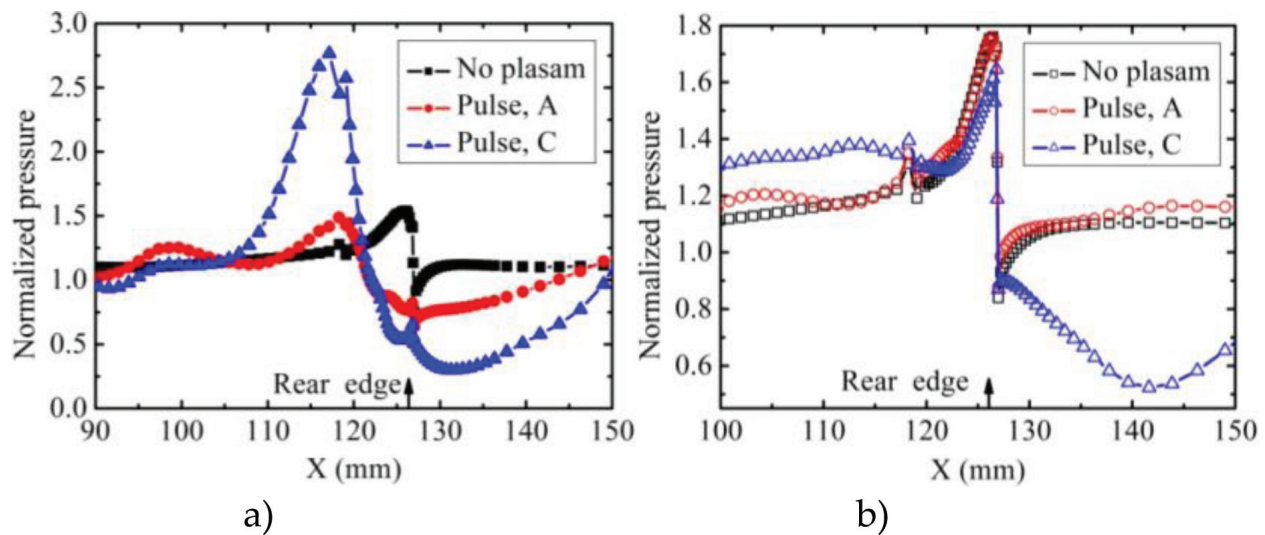
Figure 11. Wall pressure distribution near the rear edge of cavity. (a) $z = 0$ mm. (b) $z = 16$ mm.

to minimum value. But at time C, its pressure peak value is nearly 2.8 times as the no plasma case. Results about show that the original waves around the rear edge are altered which results from local combustion zone induced by the periodic disturbance of plasma and the variation of cavity shear layer.

As presented in **Figure 11b**, the wall pressure of cavity rises distinctly on $z = 16$ mm, which illuminates that the temperature goes up in the cavity. Besides, the pressure peak value at time A equals the value of the no plasma case and is lower than the value at time C. This suggests clearly that the plasma filaments can weaken the waves around the cavity rear edge during plasma actuators free period (means the actuators shutdown.), which is the same to the study of nonreaction flow [19]. Moreover, because of the effect of expansion waves (as it is known that the abrupt pressure reduction near a cavity rear edge is induced by expansion waves), the normalized pressure reduces to around0.8 and then drops in a relative gentle way until $x \approx 140.0$ mm at time C, which is due to the change of unsteady local waves and combustion.

Because the distributions of combustion products may be impacted by the change of cavity shear layer and waves, the mass fraction iso-surface of water ($Y_{H2O} = 0.05$) is shown in **Figure 12**. Firstly, around the fuel orifice for the no plasma case some water forms, but there is no water forming during the plasma actuator working duration. Secondly, compared with the no plasma case having a smooth iso-surface, the iso-surface looks wrinkled distinctly due to the influence of plasma filaments, especially in the shear layer zone. Several symmetry structures shaped like "branch pipes" can be found obviously because of plasma. The "branch pipes" generate from the front or middle part of the cavity, and then move downstream. And "branch pipes" also move upward in the process mentioned above. Hence, a "branch pipes" produced cycle is established from time A to time C. The wide extent of product water shortens in the z direction, while more water forms in the y direction at the same time.

The above phenomena can be attributed to the reasons as follows: (1) Plasma filaments existed upstream of the cavity front edge release a large amount of heat, so the local static temperature increases and then the movement of fuel jet is promoted toward upper space. Because of the
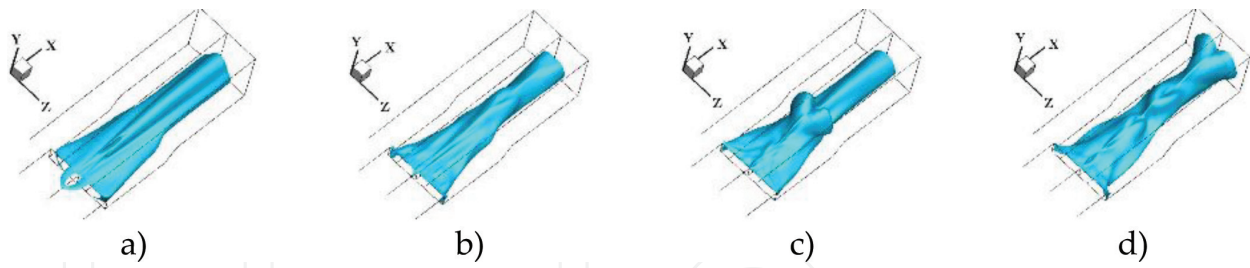
Figure 12. Iso-surface of product water, $Y_{H2O} = 0.05$: (a) no plasma; (b) with plasma, time A; (c) with plasma, time B; (d) with plasma, time C.

larger velocity far from the bottom wall (i.e., flow moves faster in the middle height of the combustor), the original product water will surely move downstream quickly. Therefore, the little water is found around the orifice when plasma actuators work, and the symmetry structures are formed in higher space downstream. It can be verified from the "branch pipes" presented in **Figure 12b–d**. (2) As stated above, the periodic fluctuation of cavity shear layer is related to the plasma filaments "cutting" effect on it, and then the mass transportation process is blocked which leads to the obvious change of combustion over the cavity. Hence, it affects the distribution of product water. Meanwhile, notice that the "branch pipes" curve structures match with the typical spanwise reverse vortex pairs in shape. Generally speaking, the spanwise reverse vortex pairs can extend the contact area between air and fuel by the methods of entraining air into its fuel core, which makes the mixing between fuel and air better and also the local combustion efficiency arisen. Whereas, the periodic disturbance from the plasma filaments impels the air and fuel transporting in the y direction. Hence, at certain periods, the efficiency of vortex pairs rises in several zones, which leads to the unsteady variation of product water, as shown in **Figure 12**. (3) The phenomena that more water forms in higher space and the less exists near the cavity mouth and combustor wall, which can be attributed to the heating effect on the whole cavity by the plasma filaments.

3.2.2. Analysis of cavity drag and mass exchange rate

The drag and mass exchange rate of cavity are two important cavity performance parameters [26]. The combustor's drag is mainly generated by the cavity as it has a nearly constant cross section. The cavity drag includes two types: pressure drag and friction drag. Pressure drag is defined as the difference value between the force on cavity front wall and rear wall. Usually, the friction drag is too small compared with pressure drag so it always can be ignored. So the pressure drag is regarded as the cavity drag here. The drag coefficient of flame holding cavity is defined as:

$$C_D = \frac{2F_D}{A\rho V^2} \tag{9}$$

where F_D is the cavity drag; A is the section area of combustor inlet; ρ is mass density; and V is velocity of inflow.

In **Table 4**, the calculation results of the cavity drag and its drag coefficient are listed. It can be observed that the drag coefficient is 0.060 at the no plasma case, which is smaller than time B

	Front wall	Rear wall	Drag	Drag coefficient
No plasma	−19.8	34.3	14.5	0.060
Plasma, A	−19.6	33.1	13.5	0.056
Plasma, B	−19.6	37.6	18.0	0.075
Plasma, C	−18.1	33.5	15.4	0.064

Table 4. Calculation results about the cavity drag, unit: N.

and C but larger than time A. In view of the change of cavity shear layer in **Figure 10**, it should be due to the moving upward of the shear layer as actuator works. As the shear layer moves upward, it deflects to the main flow and no more impacts on the cavity rear wall so the drag decreases. However, at time B and C, because of the variation of the shear layer fluctuation, stronger impact may appear the rear wall of cavity, and the combustion may be boosted in the cavity rear part, which can both lead to the increase of back pressure in the cavity. Considering the drag coefficient values at the three typical times, the time weighted average cavity drag coefficient is calculated to be 0.0668 which means the cavity drag usually increases by the plasma.

As we know, the cavity drag in reaction flow is closely related to the combustion heat release zone of a cavity. So only reducing the cavity drag may not bring benefit for the whole combustor. It can be seen that the further detail analysis about the combustion distribution in flowfield should be done to understand the effect of plasma on the cavity performance.

The mass exchange rate of cavity m' is another important parameter, which stands for the fluid mass that is inhaled into cavity from the main flow every second. The shedding vortex from cavity shear layer primary conducts the mass exchange process which can effectively inhale air and fuel into cavity and then takes them away. More shedding vortices and quicker movement can advance the flame holding ability of cavity with efficient mixing. The mass exchange rate can be analyzed by monitoring the mass flux that passes through the cavity mouth when the shear layer just covers the cavity. The mixing gas in the cavity is marked as "Y" in the unsteady flowfield at a time with stable result, and the dynamic process until all the gas "Y" leave the cavity can be observed and then the whole time involved "τ" in this process (i.e., residence time in cavity) has been recorded easily. Afterward, the mass exchange rate is $m' = m/\tau$, where m is the total mass of fluid in a cavity. Basically, the fuel exchange between internal and external of cavity is mostly affected by the interaction between the back wall and shear layer of cavity and the fuel distribution in cavity shear layer.

The mass exchange rate of cavity is given in **Table 5**. Because the species transportation is achieved through the vortices in the cavity shear layer, it is very significant for enhancing the diffusion ability of cavity shear layer. Owing to the break on the original stable structure of the shear layer resulted from the plasma filaments "cutting" effect, the mass exchange rates at plasma existing cases at times A, B, and C are 9.2, 197.2, and 107.8 times, respectively, than the "no plasma" case. In addition, the time-weighted average mass exchange rate is 8.217 g/s, which is 122.6 times than the "no plasma" case. And the variation of the mass exchange rate magnitude from time A to C is in related to fluctuation degree of cavity shear layer. As a result, the quasi-DC plasma does obviously promote the species transportation between external and internal cavity.

	No plasma	Pulse, A	Pulse, B	Pulse, C
$m^{'}$	0.067	0.614	13.013	7.223

Table 5. Calculation results of cavity mass exchange rate, unit: g/s.

3.2.3. Analysis of pressure oscillation in cavity

In the research fields related to "sound cavity," "embedded magazine" and "flame holding cavity," the dynamic study on pressure oscillation in a cavity is always greatly valued around the world [27]. According to the cavity shear layer distribution, four monitor points are chosen to capture the dynamic pressure feature, as shown in **Figure 9**. F-1 is located on the front wall of cavity with z = 16 mm (refers to a lateral section of the combustor) and F-2 is located on z = 0 mm (refers to the symmetry section of the combustor), and they are 0.5 mm beneath the front edge. R-1 is located on the rear wall with z = 16 mm and R-2 is with z = 0 mm, and they are 0.71 mm away from the rear edge. To ascertain the intensity of pressure oscillations, the sound pressure level (SPL) is used to present the time averaged pressure fluctuation magnitude, with dB as its unit, which is defined as:

$$L_{\mathrm{sp}} = 20 \log \frac{\overline{p'}}{p_{\mathrm{ref}}} \tag{10}$$

where $\overline{p'}$ and P_{ref} are the RMS of dynamic pressure and the reference sound pressure, respectively, and here P_{ref} is 2×10^{-5} Pa.

The SPLs of F-1, F-2, R-1, and R-2 are 168, 193, 188, and 191 dB, respectively. However, at the no plasma case, their SPL values are 120, 118, 124, and 106 dB, respectively. It indicates that the SPL of all the monitor points go up sharply, and the relationship between point location and magnitude of SPL changes prominently. The points are near the mouth of cavity and the effect of plasma filaments on the cavity edges is strongest, so the SPL magnitude increases here. Moreover, through the analysis on cavity drag in **Table 4**, the conclusion can be obtained that the pressure disturbance on the monitor points is controlled by combustion, and the shear layer strongly affects the change of local combustion.

In **Figure 13**, the frequency spectrum characteristics of R-1 and R-2 by FFT are depicted. The several dominant frequencies of pressure oscillation are marked with red circles here, which show that the first dominant frequency is almost the double of the plasma actuation frequency 5 kHz. Whereas, it is barely equal to the plasma actuation frequency under nonreaction condition [19]. Furthermore, nearly every dominant frequency is an integer multiple of the plasma actuation frequency. The results above indicate that the pressure oscillation in the cavity is controlled by both local combustion flowfield and the plasma actuation frequency.

3.2.4. Analysis of stagnation pressure loss and combustion efficiency

The combustor stagnation pressure recovery coefficient of time A, B, C, and the no plasma case is 0.75, 0.81, 0.65, and 0.83, respectively. And the calculated time weighted average stagnation pressure recovery coefficient is 0.73. It suggests that the overall stagnation pressure loss is
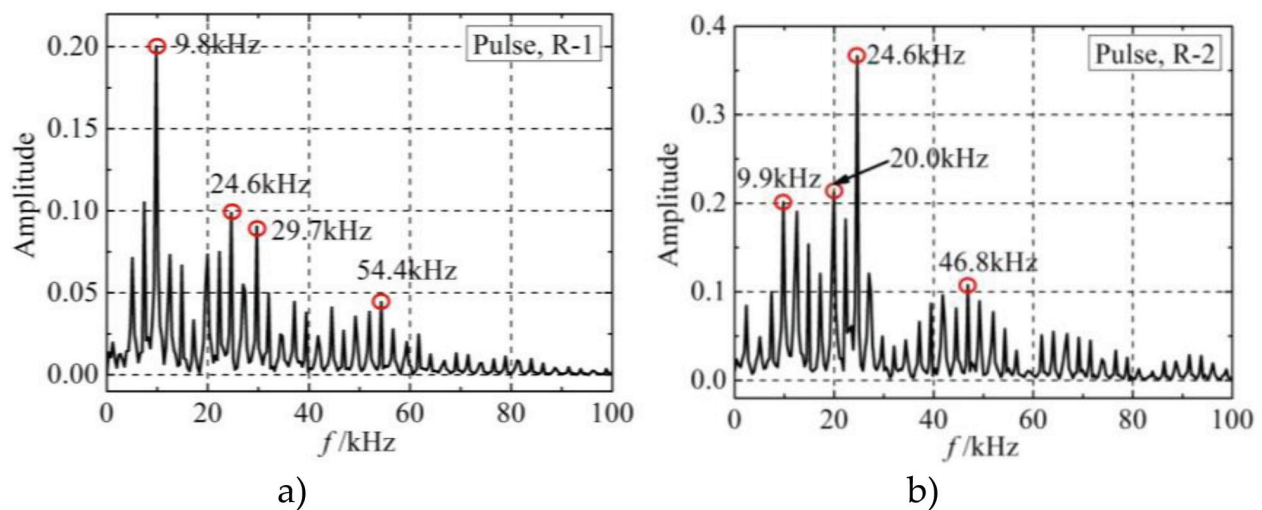
Figure 13. The normalized pressure frequency spectrum, with plasma. (a) R-1. (b) R-2.

raised due to the plasma filaments, especially for time A and C. The increase of the combustor stagnation pressure loss is caused by several factors, such as the enlargement of separation zones, the rise of back pressure induced by local combustion and the strengthening of shock waves, which is based on the analysis of cavity shear layer and wall pressure distribution.

Considering the interesting variation of product water distribution as shown in **Figure 12**, the distribution of combustion efficiency in the flow direction may also vary influenced by the plasma filaments. Hence, the combustion efficiency η_c is calculated. The distribution of combustion efficiency along x-direction is presented in **Figure 14**. Usually, the combustion efficiency goes on increasing from time A to time C due to the plasma. It can be seen the combustion efficiency of time A is little lower at most positions, but prominently higher at time B in the upstream of cavity rear wall and time C on the whole compared with the no plasma case. As involved above, the transportation ability of the spanwise reverse vortex pairs are improved by the plasma, so the local combustion efficiency during certain periods increases.

In a word, the combustion efficiency increases downstream of the front wall of cavity in most of the time due to the plasma. It becomes lower than the no plasma case at several positions for few moments, but the decrease is comparatively small. Furthermore, during one plasma cycle, the combustion efficiency gradually increases from beginning to end, which indicates that the plasma performs better during actuator free period for the pulsed actuation mode.

The ratio of power consumption of the plasma actuator to the increased combustion heat release of the combustor is calculated in value $E_f = 0.0016$ to depict the cost to effectiveness of quasi-DC plasma. Therefore, the assistance of plasma to the combustion process presents improvements in performance that outweighs the additional cost.

3.3. Conclusions

The main results are as follows: (1) Because of the "cutting" effect of quasi-DC plasma filaments, the cavity shear layer becomes fluctuating and the local combustion changes which also results
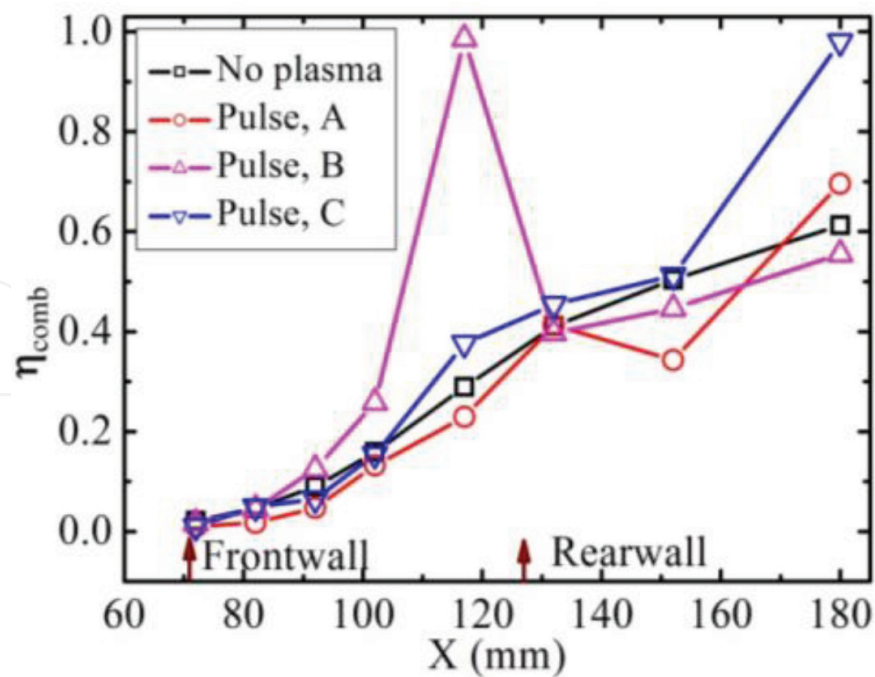
Figure 14. Combustion efficiency along *x*.

in the variation of wall pressure distribution near the cavity rear edge. On the mass fraction iso-surface of product water several "branch pipes" curve structures form periodically, which can be put down to the influence of plasma on the local combustion. (2) The effect of plasma on the cavity drag is relatively perplexing and the drag coefficient value is observed to be unsteady. Nevertheless, the mass exchange rate goes up prominently due to plasma, and the magnitude change from time A to C is in agreement with the fluctuation degree of cavity shear layer. (3) The SPLs of four cavity monitor points rise, and the frequency spectrum of monitor points near the rear edge presents that the first dominant frequency is twice the plasma actuation frequency, under the effect of plasma. Hence, the pressure oscillation in the cavity is controlled by both the plasma and local combustion flowfield. (4) On the one side, the combustion efficiency is usually increased due to plasma, and on the other side, the certain pressure loss increases resulted from the changes of combustion and waves in the flowfield by the plasma. Because the ratio of deposited plasma energy to the increased combustion heat release is extraordinarily small, it is considered that if optimal actuation parameters of the actuator are chosen the quasi-DC plasma can bring more benefits than penalties for the cavity in scramjet combustor.

Acknowledgements

Conflict of interest

The authors declared that they have no conflicts of interest to this work.

Author details

Siyin Zhou, Haiqing Wang, Wansheng Nie* and Xueke Che

*Address all correspondence to: nws1969@126.com; 286982061@qq.com

Space Engineering University, Beijing, China

References

[1] Mathur T, Gruber M, Jackson K, et al. Supersonic combustion experiments with a cavity-based fuel injector. Journal of Propulsion and Power. 2011;**17**:1305-1312

[2] Ben YA. Experimental investigation of mixing and ignition of transverse jets in supersonic crossflows [thesis]. Palo Alto: Stanford University; 2000

[3] Ding M. Research on the flame holding technology based on cavity in supersonic combustion [thesis]. Changsha: National University of Defense Technology; 2005

[4] Li G, Li H, Yang L, et al. Review of the plasma ignition and assisted combustion in Russia. Science & Technology Review. 2012;**30**:66-72

[5] Kim KM, Back SW, Han CY. Numerical study on supersonic combustion with cavity-based fuel injection. International Journal of Heat and Mass Transfer. 2004;**47**:271-286

[6] Starikovskiy A, Aleksandrov N. Plasma-assisted ignition and combustion. Progress in Energy and Combustion Science. 2013;**39**:61-110

[7] Starikovskaia SM. Plasma assisted ignition and combustion. Journal of Physics D: Applied Physics. 2006;**39**:265-299

[8] Do H, Im S, Cappelli MA, et al. Plasma assisted flame ignition of supersonic flows over a flat wall. Combustion and Flame. 2010;**157**:2298-2305

[9] Do H. Cappelli MA, Mungal G: Plasma assisted cavity flame ignition in supersonic flows. Combustion and Flame. 2010;**157**:1783-1794

[10] Leonov SB, Firsov AA, Yarantsev DA, et al. Plasma effect on shocks configuration in compression ramp. In: 17th AIAA International Space Planes and Hypersonic Systems and Technologies Conference; 11–14 April 2011. San Francisco: AIAA; 2011. pp. 2011-2362

[11] Leonov SB, Savelkin CV, Yarantsev DA, et al. Experiments on plasma-assisted combustion in M=2 hot test-bed PWT-50h. In: 46th AIAA Aerospace Sciences Meeting and Exhibit; 7–10 January 2008. Reno: AIAA; 2008. pp. 2008-1359

[12] Leonov SB, Yarantsev DA, Gromov VG, et al. Mechanisms of flow control by near-surface electrical discharge generation. In: 43rd AIAA Aerospace Sciences Meeting and Exhibit; 10–13 January 2005. Reno: AIAA; 2005. pp. 2005-2780

[13] Enloe CL, McLaughlin TE, VanDyken RD, et al. Mechanisms and responses of a single dielectric barrier plasma. In: 41st AIAA Aerospace Sciences Meeting and Exhibit; 6–9 January 2003. Reno: AIAA; 2003. pp. 2003-1021

[14] Zhou S, Nie W, Che X. Numerical modeling of quasi-dc plasma-assisted combustion for flame holding cavity. Combustion Science and Technology. 2016;**188**:1640-1654

[15] Leonov SB, Yarantsev DA, Gromov VG, et al. Mechanisms of flow near surface electrical discharge generation. Vacuum. 2006;**80**:1199-1205

[16] Cheng Y, Nie W, Li G. Numerical study of plasma aerodynamic actuation mechanism. Acta Physica Sinica. 2012;**61**:060509

[17] Wang J, Li Y, Cheng B, et al. The mechanism investigation on shock wave controlled by plasma aerodynamic actuation. Acta Physica Sinica. 2009;**58**:5513-5519

[18] Zhou S, Nie W, Che X. Numerical investigation of influence of quasi-dc discharge plasma on fuel jet in scramjet combustor. IEEE Transactions on Plasma Science. 2015;**43**:896-905

[19] Zhou S. Studies on plasma assisted combustion/flame stabilization in scramjet [thesis]. Beijing: Equipment Academy; 2014

[20] Menter FR. Two-equation eddy-viscosity turbulence models for engineering applications. AIAA Journal. 1995;**33**:1418-1425

[21] Esch DD, Siripong A, Pike RW. Thermodynamic properties in polynomial form for carbon, hydrogen, nitrogen and oxygen systems from 300 to15000°K. NASA RFL-TR-70-3 (NASA CR-111989), Nov. 1970

[22] Liou MS, Steffen CJ. A new flux splitting scheme. Journal of Computational Physics. 1993;**107**:23-39

[23] Yoon S, Jameson A. Lower-upper symmetric-gauss-Seidel method for the Euler and Navier-stokes equations. AIAA Journal. 1988;**26**:1025-1026

[24] Rajasekaran A, Babu V. Numerical simulation of three-dimensional reacting flow in a model supersonic combustor. Journal of Propulsion and Power. 2006;**22**:820-827

[25] Jiang J, Weng J. Cathode Electronics and Gas Discharge. 1st ed. Beijing: Tsinghua University Press; 1980

[26] Sun M. Studies on flow patterns and flameholding mechanisms of cavity flameholders in supersonic flows [thesis]. Changsha: National University of Defense Technology; 2008

[27] Yang D, Li J, Fan Z, et al. Investigation on aerodynamic noise characteristics of cavity flow at high subsonic speeds. Acta Aerodynamica Sinica. 2010;**28**:703-707